Mitochondrial ascorbic acid prevents mitochondrial $O_2^{\cdot-}$ formation, an event critical for U937 cell apoptosis induced by arsenite through both autophagic-dependent and independent mechanisms

Andrea Guidarelli, Silvia Carloni, Walter Balduini, Mara Fiorani, Orazio Cantoni*

Dipartimento di Scienze Biomolecolari, Università degli Studi di Urbino "Carlo Bo", 61029 Urbino, Italy

**Corresponding author*: Prof. Orazio Cantoni, Dipartimento di Scienze Biomolecolari, Sezione di Farmacologia e Farmacognosia, Università degli Studi di Urbino, Via S. Chiara 27, 61029 Urbino (PU), Italy. Tel: +39-0722-303523; Fax: +39-0722-303521; e-mail: orazio.cantoni@uniurb.it

Abbreviations: AA, L-ascorbic acid; Apo, apocynin; ATZ, 3-amino-1,2,4,-triazole; Chl, chloroquine; CsA, cyclosporin A; DHR, Dihydrorhodamine 123; DPI, diphenyleneiodonium; EB; extracellular buffer; H_2O_2, hydrogen peroxide; LC3, microtubule-associated protein light chain 3; 3-MA, 3-methyladenine; MDC, monodansylcadaverine; MPT, mitochondrial permeability transition; L-NAME, N^G-nitro-L-arginine methyl ester; NO, nitric oxide; NOX, NADPH oxidase; $O_2^{\cdot-}$, superoxide; PBS, phosphate-buffered saline; PMA, phorbol-12-myristate-13-acetate; PTIO, 2-phenyl-4,4,5,5-tetramethylimidazolin-1-oxyl-3-oxide; Rot, rotenone; Rapa, rapamycin; SVCTs, sodium-AA co-transporters.

Summary

A 16 h exposure of U937 cells to 2.5 μM arsenite promotes superoxide ($O_2^{\cdot -}$) formation and inhibition of the activity of aconitase, a $O_2^{\cdot -}$ sensitive enzyme. Both responses were abolished by the complex I inhibitor rotenone, or by the respiration-deficient phenotype. Interestingly, a similar suppressive effect was mediated by a short term pre-exposure to a low concentration of L-ascorbic acid (AA), previously shown to be actively taken up by the cells and by their mitochondria. The mitochondrial origin of $O_2^{\cdot -}$ was confirmed by fluorescence microscopy studies, whereas different approaches failed to detect a contribution of NADPH oxidase. Under similar conditions, arsenite induced autophagy as well as a decline in mitochondrial membrane potential resulting in delayed (48 h) apoptosis. Importantly, all these events turned out to be sensitive to treatments associated with prevention of $O_2^{\cdot -}$ formation, including AA, and were only partially blunted by inhibitors of autophagy. As a final note, the toxic effects mediated by $O_2^{\cdot -}$ were entirely dependent on its conversion to H_2O_2.

AA-sensitive mitochondrial $O_2^{\cdot -}$ formation is therefore involved in autophagy and apoptosis induced by arsenite in U937 cells, although part of the lethal response appears mediated by an autophagy-independent mechanism.

Keywords: Vitamin C, mitochondria, superoxide, arsenite, autophagy, apoptosis

Running Title: Mitochondrial ascorbate prevents arsenite-induced mitochondrial $O_2^{\cdot -}$ formation and autophagy-dependent and -independent apoptosis

1. Introduction

In 1994 we reported that Chinese Hamster Ovary cell variants highly resistant to hydrogen peroxide (H_2O_2) are cross-resistant to various metal compounds, including the widely diffused environmental contaminant sodium arsenite (1). In recent years, it has become increasingly clear that trivalent arsenic is indeed an oxidative stressor (2), reported to produce superoxide ($O_2^{\cdot -}$) through either NADPH oxidase (NOX) activation (3,4), or in the mitochondrial respiratory chain (5), or even at both levels with the mitochondria being downstream to NOX activation (6). Thus, although oxidative stress appears of general importance for arsenite toxicity (2,7,8), the different sources of $O_2^{\cdot -}$ in different cell types imply the possibility of the recruitment of different mechanisms of toxicity. The downstream effects/interactions of $O_2^{\cdot -}$ are indeed remarkably dependent on the intracellular microenvironment and conditions.

$O_2^{\cdot -}$ rapidly reacts with nitric oxide, when and where available, to form the highly reactive and toxic species peroxynitrite, or eventually becomes protonated to produce direct damage to diverse biological molecules, or enzymatically dismutates to H_2O_2, which then causes its deleterious effects through the intermediate formation of the highly reactive hydroxyl radical (9). The mitochondrial/extramitochondrial formation of $O_2^{\cdot -}$ is therefore compatible with direct or indirect downstream events in the same subcellular compartments in which these species are produced.

$O_2^{\cdot -}$, as a consequence of its anionic charge, cannot diffuse through biological membranes, thereby implying that the only possibility whereby mitochondrial $O_2^{\cdot -}$ may produce extramitochondrial damage is through the release of $O_2^{\cdot -}$-derived H_2O_2. This appears to be true in most circumstances, although there is a report showing that, in isolated mitochondria, some $O_2^{\cdot -}$ release may take place through voltage-dependent anion channels (10). Clearly, H_2O_2 produced *via* dismutation of NOX-derived $O_2^{\cdot -}$ can cross the mitochondrial membrane in the direction of the organelle and hence contribute to mitochondrial damage. H_2O_2 damaged mitochondria may then produce more $O_2^{\cdot-}$, thereby further fuelling the machinery leading to mitochondrial dysfunction and downstream events as autophagy as well as apoptotic or necrotic death.

Arsenite has been reported to induce autophagy in different cell types (8,11-13) and this response represents a potential determinant of the toxic effects elicited by the metalloid. In these studies, however, no attempt was made to determine the identity and source of the reactive oxygen species produced, and their involvement in the autophagic process was eventually inferred by experiments showing that an high dose of N-acetyl cysteine prevents autophagy.

These considerations lead to the conclusion that the fate and downstream effects of $O_2^{\cdot-}$ generated by arsenite exposure are conditioned by the microdomain in which the radical is produced. For similar reasons, based on the present knowledge, it is very difficult to determine the specific subcellular compartments/microdomains in which antioxidants determine their specific protective effects against arsenite-derived $O_2^{\cdot-}$. In order to provide some insight in this direction, our knowledge should be implemented by information derived from studies addressing the specific impact of the mechanism of $O_2^{\cdot-}$ formation in arsenite toxicity. Obviously we also need more information on the subcellular compartmentalization of specific antioxidants.

L-Ascorbic acid (AA) is one of the antioxidants affording cytoprotection in both cultured cells (14,15) and experimental animals exposed to arsenite (16,17). We recently performed a detailed characterization of AA uptake in U937 cells, expressing high affinity sodium-AA cotransporters (SVCT2 and 1), which allow rapid accumulation of the vitamin against its concentration gradient (18). We also obtained unexpected results providing evidence for the expression of SVCT2 in the mitochondria of these cells (19), functionally active even in the absence of Ca^{2+} and in the presence of low millimolar Na^+ concentrations, which implies their ability to concentrate the vitamin even further in these organelles (20).

We employed these cells to investigate the mechanism whereby arsenite causes apoptosis and found that this event, dependent on mitochondrial permeability transition (MPT), was prevented by a 15 min pre-exposure to as low as 10 μM AA. In addition, using different approaches, we were able to demonstrate that the mitochondrial fraction of the vitamin is entirely responsible for the observed cytoprotection (15).

Clearly, this observation is consistent with the possibility that mitochondrial $O_2^{\cdot-}$ plays a pivotal role in the specific toxicity paradigm employed, thereby suggesting that AA either prevents $O_2^{\cdot-}$ formation or directly scavenges the radical in the same site in which it is produced, in a reaction competing with $O_2^{\cdot-}$ dismutation. There are however alternative possibilities, including the one that $O_2^{\cdot-}$ is produced by NOX and that mitochondrial AA functions as an antioxidant to preserve mitochondrial function and integrity harmed by H_2O_2.

The present study fills this important gap left by our previous investigation (15) by showing that arsenite-dependent $O_2^{\cdot-}$ formation is entirely of mitochondrial origin, with hardly any contribution of the NOXs. Notably, inhibition of $O_2^{\cdot-}$ formation elicited by different manipulations was invariably associated with prevention of apoptosis. Having established a model of arsenite toxicity completely based on mitochondrial $O_2^{\cdot-}$, we then established a link between these radicals and autophagy and a further link between these events and MPT-dependent apoptosis. On the other hand, we also obtained evidence of an autophagy-independent mechanism of arsenite toxicity. An additional observation was that all the deleterious effects mediated by mitochondrial $O_2^{\cdot-}$ were attributable to the intermediate formation of H_2O_2, its dismutation product. A final important information provided by this study is that intramitochondrial AA provides cytoprotection *via* upstream inhibition of mitochondrial $O_2^{\cdot-}$ formation and hence through the prevention of both the autophagy-dependent and -independent mechanisms of toxicity.

2. Experimental Procedures

2.1 Chemicals

Sodium arsenite, AA, rotenone (Rot), diphenyleneiodonium (DPI), apocynin (Apo), phorbol-12-myristate-13-acetate (PMA), 3-methyladenine (3-MA), chloroquine (Chl), rapamycin (Rapa), catalase, 3-amino-1,2,4,-triazole (ATZ), L-methionine, 2-phenyl-4,4,5,5-tetramethylimidazolin-1-oxyl-3-oxide (PTIO), N^G-nitro-L-arginine methyl ester (L-NAME), monodansylcadaverine (MDC), Hoechst 33342, as well most reagent-grade chemicals were purchased from Sigma-Aldrich (Milan, Italy). Cyclosporin A (CsA) was purchased from Novartis (Bern, Switzerland). Dihydrorhodamine 123 (DHR), MitoSOX Red, MitoTracker Green and MitoTracker Red CMXRos were purchased from Molecular Probes (Leiden, The Netherlands).

2.2 Cell culture and treatment conditions

U937 human myeloid leukemia cells were cultured in suspension in RPMI 1640 medium (Sigma-Aldrich, Milan, Italy) supplemented with 10% fetal bovine serum (Euroclone, Celbio Biotecnologie, Milan, Italy), penicillin (100 units/ml) and streptomycin (100 μg/ml) (Euroclone), at 37 °C in T-75 tissue culture flasks (Corning Inc., Corning, NY, USA) gassed with an atmosphere of 95% air-5% CO_2. Respiration-deficient U937 cells were isolated as described in (21). Sodium arsenite was prepared as a 1 mM stock solution in saline A (8.182 g/l NaCl, 0.372 g/l KCl, 0.336 g/l $NaHCO_3$, and 0.9 g/l glucose) and stored at 4°C. Cells (1×10^5 cells/ml) were exposed to arsenite in complete RPMI 1640 culture medium, as reported in the legends to the figures. A 10 mM AA stock solution was prepared in extracellular buffer (EB, 15 mM Hepes, 135 mM NaCl, 5 mM KCl, 1.8 mM $CaCl_2$, 0.8 mM $MgCl_2$, pH 7.4) immediately before utilization. Cells (1×10^6 cells/ml) were treated with AA supplemented with 0.1 mM dithiothreitol for 15 min at 37°C in EB. Stability of AA in EB was assessed by monitoring the absorbance at 267 nm for 15 min (ε_{267} =14,600 $M^{-1}cm^{-1}$). In those experiments involving catalase depletion, U937 cells (5 × 10^6/20 ml) were incubated for 6 h at 37°C in RPMI medium containing 10 mM ATZ, an irreversible inhibitor of catalase (22).

Experiments with peroxynitrite were performed using 15 ml plastic tubes containing 5 x 10^5 cells (2 ml) of pre-warmed saline A. Peroxynitrite, synthesized as previously described (21), was rapidly added on the wall of the plastic tubes and mixed to equilibrate the peroxynitrite concentration in the culture medium. To avoid changes in pH due to the high alkalinity of the peroxynitrite stock solution, an appropriate amount of 1.5 N HCl was also added to the wall of the tubes prior to peroxynitrite.

2.3 DHR and MitoSOX Red oxidation

The cells were incubated for 30 min with 10 μM DHR, 5 μM MitoSOX Red or 0.5 μM MitoTracker Green prior to the end of the 16 h incubation with arsenite. After the treatments, the cells were washed three times and fluorescence images were captured with a BX-51 microscope (Olympus, Milan, Italy), equipped with a SPOT-RT camera unit (Diagnostic Instruments, Delta Sistemi, Rome, Italy) using an Olympus LCAch 40 x/0.55 objective lens. The excitation and emission wavelengths were 488 and 515 nm (DHR and MitoTracker Green), and 510 and 580 nm (MitoSOX Red) with a 5-nm slit width for both emission and excitation. Images were collected with exposure times of 100-400 ms, digitally acquired and processed for fluorescence determination at the single cell level on a personal computer using the J-Image software. Mean fluorescence values were determined by averaging the fluorescence values of at least 50 cells/ treatment condition/experiment.

2.4 Aconitase activity

After treatments for 16 h with arsenite, the cells were washed twice with saline A, resuspended in lysis buffer (50 mM Tris-HCl, 2 mM Na-citrate, 0.6 mM $MnCl_2$, pH 7.4) and finally sonicated three times on ice by using the Sonicator Ultrasonic Liquid Processor XL (Heat System-Ultrasonics, Inc., NY) operating at 20 W (30 sec). The resulting homogenates were centrifuged for 5 min at 18,000 x g at 4°C. Aconitase activity was determined spectrophotometrically in the supernatants at 340 nm, as described by Gardner (23).

2.5 Cytotoxicity assay

After treatments with arsenite, the number of viable cells was estimated with the trypan blue exclusion assay. Briefly, an aliquot of the cell suspension was diluted 1:2 (v/v) with 0.4% trypan blue and the viable cells (*i.e.*, those excluding trypan blue) were counted with the hemocytometer.

2.6 Apoptosis detection

After treatments, the cells were incubated for 5 min with the cell-permeable DNA dye (Hoechst 33342, 10 μmol/l) and then visualized by a fluorescence microscope to assess nuclear morphology (chromatin condensation and fragmentation). Cells with homogeneously stained nuclei were considered viable. Apoptotic DNA fragmentation in individual cells was also detected by using the comet assay (24). After the treatments, the cells were resuspended at 2.0×10^4 cells/100 μl in 1.0% low-melting agarose in phosphate buffer saline (PBS, 8 g/l NaCl, 1.15 g/l Na_2HPO_4, 0.2 g/l KH_2PO_4, 0.2 g/l KCl) containing 5 mM EDTA and immediately pipetted into agarose-coated slides. The slides were immersed in ice-cold lysing solution (2.5 M NaCl, 100 mM EDTA, 10 mM

Tris, 1% sarkosyl, 5% dimethyl sulfoxide, and 1% Triton X-100, pH 10.0) for 60 min. The slides were placed on an electrophoresis tray with an alkaline buffer (300 mM NaOH and 1 mM EDTA) and left for 20 min to allow the DNA to unwind; electrophoresis was then performed at 300 mA for 20 min in the same alkaline buffer maintained at 14 °C. The slides were subsequently washed and stained with ethidium bromide. The DNA was visualized by a fluorescence microscope. Mean fluorescence values were determined by averaging the fluorescence values of at least 50 cells/treatment condition/experiment.

2.7 Measurement of mitochondrial membrane potential

The cells were incubated for 30 min with 50 nM MitoTracker Red CMXRos prior to the end of the 16 h incubation with arsenite. After treatments, the cells were washed three times and analyzed by a fluorescence microscope. The resulting images were taken and processed as described above. The excitation and emission wavelengths were 545 and 610 nm, respectively, with a 5-nm slit width for both emission and excitation. Images were collected with exposure times of 100-400 ms, digitally acquired and processed for fluorescence determination at the single cell level on a personal computer using the J-Image software. Mean fluorescence values were determined by averaging the fluorescence values of at least 50 cells/treatment condition/experiment.

2.8 MDC staining

The cells were incubated for 30 min with 50 μM MDC prior to the end of the 36 h incubation with arsenite. After treatments, the cells were washed three times and analyzed by a fluorescence microscope. The excitation and emission wavelengths were 360 and 525 nm, respectively, with a 5-nm slit width for both emission and excitation.

Images were collected with exposure times of 100-400 ms, digitally acquired on a personal computer using the J-Image software.

2.9 Western blot analysis

After treatments, the cells were washed twice with PBS and incubated on ice for 1 h with the lysis buffer (50 mM Tris, 5 mM EDTA, 150 mM NaCl, 0.5% Nonidet P-40, 1 mM phenylmethylsulfonyl fluoride, 1 mM sodium vanadate, and 1 mM sodium fluoride, pH 7.4). The cells were then homogenized by sonication for three times (30 sec) on ice and finally centrifuged at 21,500 g for 10 min at 4°C to remove detergent-insoluble material. Supernatants were assayed for protein concentration using the Bio-Rad protein assay reagent. Equal amounts of total protein were separated by 10% and 15% gel electrophoresis and electrophoretically transferred to PVDF membranes. ColorBurst^{TM}eletctrophoresis marker (3 µl/gel, Sigma, C1992) was used for qualitative molecular mass determinations and for visual confirmation of blot transfer efficiency. Then, blots were blocked with non-fat dry milk in TBS-T (10 mM Tris, 150 mM NaCl, pH 7.6, plus 0.1% Tween-20) and probed with the following primary antibodies: anti-microtubule-associated protein light chain 3 (LC3) (1:1000, polyclonal; Cell Signaling Technology, #2775) and anti-p62 (1:1000, monoclonal; Abcam, ab56416). Immunoblots were processed with horseradish peroxidase-conjugated anti-rabbit or anti-mouse antibody (1:4000, Santa Cruz Biotechnology) and detected using the enhanced chemiluminescence (ECL) system (Amersham Pharmacia Biotech). A monoclonal antibody against β-actin (1:4000, Santa Cruz Biotechnology, sc-8432) was used as control for protein gel loading. Blots were analyzed using the J-Image software. Data were normalized to those of β-actin and expressed as % of control.

2.10 Immunofluorescence analysis

After treatments, the cells were incubated for 30 min in 2 ml of saline A in 35-mm tissue culture dishes containing an uncoated coverslip. Under these conditions, cells rapidly attach to the coverslip. The cells were then fixed for 1 min with 95% ethanol/5% acetic acid, washed with PBS and blocked in PBS containing bovine serum albumin (2% w/v) for 30 min at room temperature. The cells were subsequently incubated with rabbit polyclonal cleaved anti-caspase-3 antibody (1:250 in PBS containing 2% bovine serum albumin; Cell Signaling Technology, #9661), in other experiments the cells were incubated with rabbit polyclonal anti-nitrotyrosine antibody (1:100 in PBS containing 2% bovine serum albumin, Upstate Biotechnology, #06-284) stored for 18 h at 4 °C, washed and then exposed to fluorescein isothiocyanate (FITC, Santa Cruz Biotechnology)-conjugated secondary antibodies diluted 1/100 in PBS for 2 h in the dark. Stained cells were captured by a fluorescence microscope and the resulting images were processed for fluorescence determination as described above.

2.11 Statistical analysis

The results are expressed as means ± SD. Statistical differences were analyzed by one-way ANOVA followed by Dunnett's test for multiple comparison or two-way ANOVA followed by Bonferroni's test for multiple comparison. A value of $P < 0.05$ was considered significant.

3. Results

3.1 Mitochondrial superoxide formation

U937 cells were exposed for 16 h to 2.5 μM arsenite and subsequently loaded with MitoSOX Red, a fluorochrome commonly employed for the detection of $O_2^{\cdot-}$, the immediate precursor of H_2O_2, in the mitochondria of live cells (25). As it can be appreciated from the image shown in Fig. 1A, the fluorescence response mediated by arsenite is punctuate, as in the case of cells loaded with MitoTracker Green, a mitochondrial marker, and indeed the merge image provides evidence of colocalization of the two fluorochromes.

Consistent with the mitochondrial origin of $O_2^{\cdot-}$ are the results showing that the fluorescence response elicited by arsenite is prevented by Rot, a complex I inhibitor, as well as by the respiration-deficient phenotype (Fig. 1B). Finally, evidence of Rot or respiration-deficient phenotype sensitive inhibition of aconitase activity was also obtained (Fig. 1C). Although inhibition of aconitase activity is commonly considered as a marker of both mitochondrial and cytoplasmic $O_2^{\cdot-}$ formation, the observed sensitivity to Rot, or the respiration-deficient phenotype, implies that mitochondria represent the main source from which these radicals are being generated.

Coherently, two well established NADPH oxidase inhibitors, Apo and DPI (26), failed to affect the MitoSOX Red-dependent fluorescence response elicited by arsenite (Fig. 1B) and similar results were obtained in experiments measuring aconitase activity (Fig. 1C).

In other experiments MitoSOX Red was replaced with DHR, a fluorescence probe allowing detection of radical species, including $O_2^{\cdot-}$, in both the mitochondrial and extramitochondrial compartments (27). Once again, arsenite induced a fluorescence response sensitive to Rot, or the respiration-deficient phenotype, albeit insensitive to Apo or DPI (Fig. 1D). A significant fluorescence signal was also detected after treatment with

PMA, a well established stimulus for NADPH oxidase activity (28), and this response was insensitive to rotenone and abolished by Apo, or DPI (Fig. 1E). An analogous fluorescence response was observed using respiration-deficient cells, with an identical sensitivity to Apo and DPI and insensitivity to Rot (Fig. 1F).

Collectively, these results indicate that in U937 cells arsenite promotes $O_2^{\cdot -}$ formation in mitochondria, with hardly any contribution of NADPH oxidase.

3.2 Induction of autophagy

We analysed whether exposure to arsenite causes authophagy in the specific toxicity paradigm employed. For this purpose, U937 cells were exposed for increasing time intervals to 2.5 μM arsenite and then processed to determine the levels of LC3-II, a hallmark protein of authophagy (29). A slightly enhanced LC3-II expression was detected after 16 or 24 h (not shown) and an even greater response was obtained at the 36 h time point (Fig. 2A). Under identical conditions, reduced expression of p62 (an additional biomarker of autophagy, 29) was also detected (Fig. 2B). Finally, exposure to arsenite caused autophagosome formation, as measured by MDC staining (Fig. 2C).

Collectively, these results indicate that arsenite triggers an autophagic process in cultured U937 cells.

3.3 Prevention of mitochondrial superoxide formation suppresses autophagy

We first determined the effect of Rot on arsenite-induced autophagy. As previously demonstrated (Fig. 1B-D), Rot suppresses mitochondrial $O_2^{\cdot -}$ formation and, under identical conditions, also abolished the effects of arsenite on LC3-II (Fig. 2A) and p62 expression (Fig. 2B) as well as on the process of autophagosome formation (Fig. 2C). Rot alone failed to produce effects in the absence of additional treatments.

These results indicate that arsenite triggers events associated with mitochondrial $O_2^{\cdot-}$ formation, which in turns leads to autophagy. In order to determine a possible link with cytotoxicity, we first analysed the effect of 3-MA (or Chl) and Rapa, respectively inhibiting (30,31) or stimulating (32) autophagosome formation, on the kinetics of U937 cell proliferation in the presence of arsenite. While the inhibitors produced very little effect, or none, in the absence of arsenite (Fig. 3A), 3-MA (or Chl) virtually suppressed, and Rapa remarkably enhanced, the fluorescence associated with autophagosome formation (Fig. 3A). There was a significant impact also on the number of viable cells detected after 16-48 h of arsenite exposure, significantly increased, or decreased, by 3-MA (or Chl) and Rapa, respectively (Fig. 3B).

Collectively, these results indicate that authophagy induced by arsenite is entirely mediated by species derived from mitochondrial $O_2^{\cdot}$. In addition, autophagy appeared to mediate at least part of the cytotoxicity elicited by arsenite.

3.4 Prevention of mitochondrial superoxide formation and autophagy promotes survival

We reproduced some recent results obtained in our laboratory (15) indicating that arsenite causes an early (16 h) decline in mitochondrial membrane potential sensitive to the MPT inhibitor CsA (Fig. 4A). This observation is consistent with the notion that the metalloid induces MPT-dependent toxicity, and indeed CsA provided cytoprotection over the 48 h of exposure to the metalloid (Fig. 4B). We also noticed that some of the arsenite-treated cells present typical signs of apoptosis, as cell shrinkage or blebbing. Coherently, we found that these cells express active caspase 3 (28%, not shown) as well as fragmented chromatin, assayed morphologically (Fig. 4C) or by single-cell gel electrophoresis (Fig. 4D). CsA suppressed all these effects.

Additional experiments showed that the effects of arsenite on mitochondrial membrane potential (Fig. 4A), cell viability (Fig. 4B) and apoptotic chromatin fragmentation (Fig. 4C and D) are prevented by Rot as well as by the respiration-deficient phenotype. Interestingly, 3-MA or Chl, while suppressing autophagosome formation only partially mitigated these effects.

Taken together, the above results indicate that arsenite causes U937 cell apoptosis *via* a MPT-dependent mechanism mediated by mitochondrial $O_2^{.-}$ formation. We also obtained indirect evidence suggesting that autophagy is only partially associated with apoptosis induced by the metalloid.

3.5 Mitochondrial superoxide formation elicited by arsenite is linked to toxicity by the intermediate formation of H_2O_2, in the absence of apparent formation, or effects, of peroxynitrite

It is well established that mitochondrial $O_2^{.-}$ cannot escape mitochondria (33,34). Its formation is therefore associated with its rapid dismutation to H_2O_2, an event favoured by manganese superoxide dismutase. The latter can then react further with divalent iron within these organelles to produce hydroxyl radical species, or eventually diffuse in the cytosol or even in the nucleus to produce therein its indirect deleterious effects. The occurrence and relevance of these events were assessed in experiments in which the cells were challenged with arsenite in the absence or presence of catalase. As indicated in Table 1 enzymatically active catalase, unlike the boiled enzyme, prevented the DHR fluorescence response and toxicity elicited by the metalloid. Coherently ATZ supplementation, while causing an about 70% reduction in catalase activity (not shown), remarkably enhanced arsenite-dependent DHR oxidation and toxicity.

These results indicate that arsenite-dependent toxicity attributable to mitochondrial $O_2^{.-}$ is entirely mediated by the intermediate formation of H_2O_2. This observation therefore rules out other possible interactions of $O_2^{\cdot -}$ with NO to generate peroxynitrite. As this event has been observed in other cell types (5,35,36), we nevertheless performed experiments measuring nitrotyrosine immunoreactivity (Table 2). This event was readily observed after exposure to reagent peroxynitrite and was suppressed by L-methionine, a scavenger of this reactive nitrogen species (37). On the other hand, treatment with arsenite failed to produce detectable nitrotyrosine immunoreactivity. The results illustrated in Table 2 also indicate that L-methionine, the NO synthase inhibitor L-NAME (38) or the NO scavenger PTIO (39) fail to prevent arsenite toxicity.

Taken together, the above results indicate that U937 cell death mediated by arsenite is dependent on the early mitochondrial formation of $O_2^{\cdot -}$ and by its downstream dismutation to H_2O_2, with no evidence of relevant peroxynitrite formation.

3.6 Cytoprotection by mitochondrial ascorbate is associated with upstream events leading to prevention of mitochondrial superoxide formation

We first showed that AA is as effective as Rot, or the respiration-deficient phenotype, in preventing mitochondrial $O_2^{\cdot -}$ formation (Fig. 1B-D). These results were then implemented by the demonstration of an AA-mediated prevention of autophagy (Fig. 2) and loss of mitochondrial membrane potential (Fig. 4A). The vitamin also suppressed the MPT-dependent toxicity elicited by arsenite, as measured as number of viable cells (Fig. 4B), cells expressing active caspase 3 (not shown) or cells with fragmented chromatin by two independent assays (Fig. 4C and D). As a final note, AA alone failed to produce effects in the absence of additional treatments.

These results imply that intramitochondrial AA blunts arsenite toxicity *via* a mechanism associated with inhibition of $O_2^{\cdot -}$ formation, which in turn leads cells to autophagy-dependent and -independent mechanisms converging in MPT-dependent apoptosis.

4. Discussion

The present study shows that arsenite selectively triggers the mitochondrial formation of $O_2^{\cdot-}$ in cultured U937 cells. This notion was established with the following observations: i) the MitoSOX-Red fluorescence response evoked by arsenite, indicative of $O_2^{\cdot-}$ formation, co-localizes with a mitochondrial marker (Fig. 1A); ii) the same fluorescence response was suppressed by the complex one inhibitor Rot and by the respiration-deficient phenotype, with hardly any effect observed using the NOX inhibitors DPI or Apo (Fig. 1B); iii) arsenite inhibited aconitase activity, an enzyme predominantly mitochondrial and susceptible to $O_2^{\cdot-}$-dependent inhibition (40,41). Inhibition of aconitase activity was indeed suppressed by treatments/conditions preventing $O_2^{\cdot-}$ formation (Fig. 1C).

These results are therefore in keeping with the notion that $O_2^{\cdot-}$ is produced at the mitochondrial level and suggest that the contribution of NOX is either negligible or absent. In order to further address this second point, we performed experiments with DHR, which produces responses indicative of $O_2^{\cdot-}$ formation (as well as of other radical species) in both the mitochondrial and extramitochondrial compartments (27). We first showed that arsenite evokes a DHR-fluorescence response characterised by the same inhibitor sensitivity previously obtained with MitoSOX-Red (Fig. 1B). Under the same conditions, PMA was employed to obtain a DHR-fluorescence response sensitive to DPI, or Apo, and insensitive to Rot in both respiration-proficient (Fig. 1E) and -deficient (Fig. 1F) cells.

The first point we can make is that, in U937 cells, in which NOX activity is proficiently activated by PMA, arsenite preferentially targets mitochondria to selectively trigger events associated with mitochondrial $O_2^{\cdot-}$ formation. In addition, all the downstream effects induced by $O_2^{\cdot-}$ appeared entirely dependent on the formation of H_2O_2

(Table 1), with hardly any contribution of peroxynitrite (Table 2), whose formation requires parallel $O_2^{\cdot-}$ and NO release and availability.

The observation that a short-term pre-exposure to 10 μM AA was as effective as Rot, or the respiration-deficient phenotype, in preventing $O_2^{\cdot-}$ formation allow us to draw a second conclusion. Having previously demonstrated (15) that the mitochondrial fraction of AA is entirely responsible for cytoprotection against arsenite, it appears reasonable to suggest that the vitamin is involved in the regulation/inhibition of early mitochondrial events associated with $O_2^{\cdot-}$ formation and/or in its direct scavenging. It is important to remind that in these experiments the cells were treated with AA supplemented with 0.1 mM dithiothreitol for 15 min at 37°C in EB, a condition preventing the extracellular oxidation of the vitamin.

We subsequently measured conventional parameters indicative of autophagy, as LC3-II (Fig. 2A) or p62 expression (Fig. 2B), or autophagosome formation (Fig. 2C), and demonstrated their sensitivity to Rot, or the respiration-deficient phenotype, thereby emphasising the notion that these events are downstream to $O_2^{\cdot-}$ formation. In other words arsenite appears to induce autophagy *via* the intermediate formation of $O_2^{\cdot-}$. AA, by preventing $O_2^{\cdot-}$ formation, also suppressed autophagy.

These results imply a pro-death role of autophagy and indeed we were able to show that 3-MA (or Chl), or Rapa, respectively suppress, or enhance, the effects of arsenite on autophagosome formation (Fig. 3A). The number of viable cells detected after a 48 h time interval of arsenite exposure was enhanced by 3-MA or Chl and reduced by Rapa (Fig. 3B). We then went on to demonstrate that arsenite causes loss of mitochondrial membrane potential sensitive to CsA (Fig 4A), in keeping with our previous findings indicating that the metalloid leads to MPT (15). AA mimicked the effects of CsA. Experiments using rot or respiration-deficient cells provided identical results whereas 3-MA, or Chl, reduced -but did not abolish- loss of mitochondrial membrane potential induced by arsenite (Fig. 4A).

The results thus far discussed imply a role for autophagy, and strongly suggest the additional involvement of an autophagy-independent mechanism, in MPT-dependent arsenite toxicity. Both mechanisms appear downstream to mitochondrial $O_2^{\cdot-}$ formation. Our final approach was to provide further experimental ground for this notion. We measured the number of viable (Fig. 4B) and apoptotic (Fig. 4C and D) cells and showed that arsenite toxicity is sensitive to manipulations preventing $O_2^{\cdot-}$ formation, i.e. Rot, the respiration-deficient phenotype or AA. The vitamin also suppressed activation of caspase 3 mediated by arsenite (not shown). 3-MA (or Chl), however, only partially reduced arsenite induced loss of viability (Fig. 4B) and apoptosis (4C and D).

Taken together, the above results indicate that arsenite selectively triggers events associated with the mitochondrial formation of $O_2^{\cdot-}$. These radicals dismutate to H_2O_2, presumably in the mitochondria, in which the oxidant produces time-dependent damage through the intermediate formation of hydroxyl radical species. Part of the H_2O_2 produced exits the mitochondria, thereby triggering autophagy and downstream events fostering the mitochondrial dysfunction. MPT resulting from either direct effects of intramitochondrial H_2O_2, or by these effects combined with autophagy, subsequently leads to apoptosis. The cytoprotective effects of AA are then readily explained on the bases of the mitochondrial compartmentalization of the vitamin (15) and on its ability to directly scavenge $O_2^{\cdot-}$ or prevent its mitochondrial formation.

In conclusion, the present study establishes a link between autophagy and toxicity induced by arsenite in a model entirely dependent on mitochondrial $O_2^{\cdot-}$ formation, mediated by events sensitive to mitochondrial AA (15). However, it appears that the lethal response evoked by the metalloid is also associated with autophagy-independent events once again downstream to mitochondrial $O_2^{\cdot-}$ formation and hence sensitive to AA.

Conflict of interest

The authors declare that they have no conflict of interest.

Acknowledgements

This Research was supported by Ministero dell'Università e della Ricerca Scientifica e Tecnologica, Programmi di Ricerca Scientifica di Rilevante Interesse Nazionale, 2010-2011, (Grant number: 20108YB5W3-001, O.C.).

References

[1] Cantoni, O., Hussain, S., Guidarelli, A., and Cattabeni, F. (1994) Cross-resistance to heavy metals in hydrogen peroxide-resistant CHO cell variants. *Mutat. Res.* **324,** 1-6.

[2] Flora, S. J. (2011) Arsenic-induced oxidative stress and its reversibility. *Free Radic. Biol. Med.* **51,** 257-281.

[3] Smith, K. R., Klei, L. R., and Barchowsky, A. (2001) Arsenite stimulates plasma membrane NADPH oxidase in vascular endothelial cells. *Am. J. Physiol. Lung. Cell Mol. Physiol.* **280,** L442-449.

[4] Straub, A. C., Clark, K. A., Ross, M. A., Chandra, A. G., Li, S., et al. (2008) Arsenic-stimulated liver sinusoidal capillarization in mice requires NADPH oxidase-generated superoxide. *J. Clin. Invest.* **118,** 3980-3989.

[5] Liu, S. X., Davidson, M. M., Tang, X., Walker, W. F., Athar, M., et al. (2005) Mitochondrial damage mediates genotoxicity of arsenic in mammalian cells. *Cancer Res.* **65,** 3236-3242.

[6] Li, Y. N., Xi, M. M., Guo, Y., Hai, C. X., Yang, W. L., et al. (2014) NADPH oxidase-mitochondria axis-derived ROS mediate arsenite-induced HIF-1alpha stabilization by inhibiting prolyl hydroxylases activity. *Toxicol. Lett.* **224,** 165-174.

[7] Wang, Y., Xu, Y., Wang, H., Xue, P., Li, X., et al. (2009) Arsenic induces mitochondria-dependent apoptosis by reactive oxygen species generation rather than glutathione depletion in Chang human hepatocytes. *Arch. Toxicol.* **83,** 899-908.

[8] Gong, X., Ivanov, V. N., Davidson, M. M., and Hei, T. K. (2015) Tetramethylpyrazine (TMP) protects against sodium arsenite-induced nephrotoxicity by suppressing ROS production, mitochondrial dysfunction, pro-inflammatory signaling pathways and programed cell death. *Arch. Toxicol.* **89,** 1057-1070.

[9] Beckman, J. S. and Koppenol, W. H. (1996) Nitric oxide, superoxide, and peroxynitrite: the good, the bad, and ugly. *Am. J. Physiol.* **271,** C1424-1437.

[10] Han, D., Antunes, F., Canali, R., Rettori, D., and Cadenas, E. (2003) Voltage-dependent anion channels control the release of the superoxide anion from mitochondria to cytosol. *J. Biol. Chem.* **278,** 5557-5563.

[11] Bolt, A. M., Zhao, F., Pacheco, S., and Klimecki, W. T. (2012) Arsenite-induced autophagy is associated with proteotoxicity in human lymphoblastoid cells. *Toxicol. Appl. Pharmacol.* **264,** 255-261.

[12] Zhu, X. X., Yao, X. F., Jiang, L. P., Geng, C. Y., Zhong, L. F., et al. (2014) Sodium arsenite induces ROS-dependent autophagic cell death in pancreatic beta-cells. *Food Chem. Toxicol.* **70,** 144-150.

[13] Teng, Y. C., Tai, Y. I., Huang, H. J., and Lin, A. M. (2015) Melatonin Ameliorates Arsenite-Induced Neurotoxicity: Involvement of Autophagy and Mitochondria. *Mol. Neurobiol*. **52,** 1015-1022.

[14] Bera, A. K., Rana, T., Das, S., Bandyopadhyay, S., Bhattacharya, D., et al. (2010) L-Ascorbate protects rat hepatocytes against sodium arsenite--induced cytotoxicity and oxidative damage. *Hum. Exp. Toxicol.* **29,** 103-111.

[15] Guidarelli, A., Fiorani, M., Azzolini, C., Cerioni, L., Scotti, M., et al. (2015) U937 cell apoptosis induced by arsenite is prevented by low concentrations of mitochondrial ascorbic acid with hardly any effect mediated by the cytosolic fraction of the vitamin. *BioFactors* **41,** 101-110.

[16] Ramanathan, K., Anusuyadevi, M., Shila, S., and Panneerselvam, C. (2005) Ascorbic acid and alpha-tocopherol as potent modulators of apoptosis on arsenic induced toxicity in rats. *Toxicol. Lett.* **156,** 297-306.

[17] Singh, S. and Rana, S. V. (2010) Ascorbic acid improves mitochondrial function in liver of arsenic-treated rat. *Toxicol. Ind. Health.* **26,** 265-272.

[18] Azzolini, C., Fiorani, M., Guidarelli, A., and Cantoni, O. (2011) Studies with low micromolar levels of ascorbic and dehydroascorbic acid fail to unravel a preferential route for vitamin C uptake and accumulation in U937 cells. *Br. J. Nutr.* **28,** 1-6.

[19] Azzolini, C., Fiorani, M., Cerioni, L., Guidarelli, A., and Cantoni, O. (2013) Sodium-dependent transport of ascorbic acid in U937 cell mitochondria. *IUBMB Life* **65,** 149-153.

[20] Fiorani, M., Azzolini, C., Cerioni, L., Scotti, M., Guidarelli, A., et al. (2015) The mitochondrial transporter of ascorbic acid functions with high affinity in the presence of low millimolar concentrations of sodium and in the absence of calcium and magnesium. *Biochim. Biophys. Acta* **1848,** 1393-1401.

[21] Guidarelli, A., Tommasini, I., Fiorani, M., and Cantoni, O. (2000) Essential role of the mitochondrial respiratory chain in peroxynitrite-induced strand scission of genomic DNA. *IUBMB Life* **50,** 195-201.

[22] Darr, D. and Fridovich, I. (1986) Irreversible inactivation of catalase by 3-amino-1,2,4-triazole. *Biochem. Pharmacol.* **35,** 3642.

[23] Gardner, P. R. (2002) Aconitase: sensitive target and measure of superoxide. *Methods Enzymol.* **349,** 9-23.

[24] Singh, N. P., McCoy, M. T., Tice, R. R., and Schneider, E. L. (1988) A simple technique for quantitation of low levels of DNA damage in individual cells. *Exp. Cell Res.* **175,** 184-191.

[25] Mukhopadhyay, P., Rajesh, M., Hasko, G., Hawkins, B. J., Madesh, M., et al. (2007) Simultaneous detection of apoptosis and mitochondrial superoxide production in live cells by flow cytometry and confocal microscopy. *Nat. Protoc.* **2,** 2295-2301.

[26] Brandes, R. P., Weissmann, N., and Schroder, K. (2014) Nox family NADPH oxidases: Molecular mechanisms of activation. *Free Radic. Biol. Med.* **76,** 208-226.

[27] Gomes, A., Fernandes, E., and Lima, J. L. (2005) Fluorescence probes used for detection of reactive oxygen species. *J. Biochem. Biophys. Methods* **65,** 45-80.

[28] Abramov, A. Y., Jacobson, J., Wientjes, F., Hothersall, J., Canevari, L., et al. (2005) Expression and modulation of an NADPH oxidase in mammalian astrocytes. *J. Neurosci.* **25,** 9176-9184.

[29] Johansen, T. and Lamark, T. (2011) Selective autophagy mediated by autophagic adapter proteins. *Autophagy* **7,** 279-296.

[30] Wu, Y. T., Tan, H. L., Shui, G., Bauvy, C., Huang, Q., et al. (2010) Dual role of 3-methyladenine in modulation of autophagy via different temporal patterns of inhibition on class I and III phosphoinositide 3-kinase. *J. Biol. Chem.* **285,** 10850-10861.

[31] Klionsky, D. J. Abdalla, F. C. Abeliovich, H. Abraham, R. T. Acevedo-Arozena, A., et al. (2012) Guidelines for the use and interpretation of assays for monitoring autophagy. *Autophagy* **8,** 445-544.

[32] Brown, E. J., Albers, M. W., Shin, T. B., Ichikawa, K., Keith, C. T., et al. (1994) A mammalian protein targeted by G1-arresting rapamycin-receptor complex. *Nature* **369**, 756-758.

[33] Murphy, M. P. (2009) How mitochondria produce reactive oxygen species. *Biochem. J.* **417,** 1-13.

[34] Stowe, D. F. and Camara, A. K. (2009) Mitochondrial reactive oxygen species production in excitable cells: modulators of mitochondrial and cell function. *Antioxid. Redox. Signal.* **11,** 1373-1414.

[35] Bunderson, M., Coffin, J. D., and Beall, H. D. (2002) Arsenic induces peroxynitrite generation and cyclooxygenase-2 protein expression in aortic endothelial cells: possible role in atherosclerosis. *Toxicol. Appl. Pharmacol.* **184,** 11-18.

[36] Wang, F., Zhou, X., Liu, W., Sun, X., Chen, C., et al. (2013) Arsenite-induced ROS/RNS generation causes zinc loss and inhibits the activity of poly(ADP-ribose) polymerase-1. *Free Radic. Biol. Med.* **61,** 249-256.

[37] Pryor, W. A., Jin, X., and Squadrito, G. L. (1994) One- and two-electron oxidations of methionine by peroxynitrite. *Proc. Natl. Acad. Sci. U S A* **91,** 11173-11177.

[38] Knowles, R. G. and Moncada, S. (1994) Nitric oxide synthases in mammals. *Biochem. J.* **298,** 249-258.

[39] Maeda, H., Akaike, T., Yoshida, M., and Suga, M. (1994) Multiple functions of nitric oxide in pathophysiology and microbiology: analysis by a new nitric oxide scavenger. *J. Leukoc. Biol.* **56,** 588-592.

[40] Yan, L. J., Levine, R. L., and Sohal, R. S. (1997) Oxidative damage during aging targets mitochondrial aconitase. *Proc. Natl. Acad. Sci. U S A* **94,** 11168-11172.

[41] Scandroglio, F., Tortora, V., Radi, R., and Castro, L. (2014) Metabolic control analysis of mitochondrial aconitase: influence over respiration and mitochondrial superoxide and hydrogen peroxide production. *Free Radic. Res.* **48,** 684-693.

Legends to the figures

Fig 1. Arsenite promotes AA-sensitive mitochondrial $O_2^{\cdot-}$ formation.

(A) Representative microscope images of cells exposed for 16 h to 2.5 μM arsenite and treated in the final 30 min with MitoSOX Red and MitoTracker Green. In the merged image (overlay), regions containing both MitoSOX-Red and MitoTracker Green fluorescence appear yellow. (B-D) Cells were exposed for 15 min to 0.5 μM Rot, 1 μM DPI or 10 μM Apo and incubated for a further 16 h with arsenite. In alternative, cells were pretreated for 15 min with 10 μM AA in EB and the exposed to arsenite (16 h) in fresh culture medium. In selected experiments, arsenite was given to respiration-deficient (RD) cells. After treatments, the cells were analyzed for MitoSOX Red-fluorescence (B), aconitase activity (C) and DHR-fluorescence (D). (E and F) Respiration-proficient (RP) or RD cells were exposed for 15 min to DPI, Apo or Rot and subsequently treated for 30 min with 100 μg/ml PMA. After treatments, the cells were analyzed for DHR-fluorescence. Results represent the means ± SD calculated from at least 3 separate experiments. **P* < 0.01, as compared to untreated cells (one-way ANOVA followed by Dunnet's test).

Fig 2. Arsenite-dependent mitochondrial $O_2^{\cdot-}$ formation triggers autophagy through a mechanism sensitive to AA.

(A) Cells were exposed to AA or Rot, as indicated in the legend to Fig. 1B, and subsequently treated for 36 h with arsenite. After treatments, the cells were processed for Western blot analysis using an antibody against either LC3 or p62. β-Actin was used as an equal loading control. (B) Relative amounts of LC3 or p62 were quantified by densitometric analysis and expressed as % of control (untreated). Blots shown are representative of 3 separate experiments with similar outcomes. Results represent the means ± SD calculated from three to five separate experiments. **P* < 0.01, as compared to untreated cells (one-way ANOVA followed by Dunnet's test). (C) Autophagic vacuoles were observed by fluorescent microscopy of MDC staining. Arrows indicate the cells that containing autophagic vacuoles.

Fig 3. Effects of 3-MA, Chl or Rapa on arsenite-induced autophagy and toxicity.

(A) Cells were pre-exposed to 1 mM 3-MA (1h), 10 µM Chl (1 h) or 100 nM Rapa (4 h) and subsequently grown for an additional 36 h in the presence of arsenite. After treatments, the cells were analyzed for MDC staining. (B) Counts of cells exposed for increasing time intervals to arsenite in with or without addition of 3-MA, Chl or Rapa. Results represent the means ± SD calculated from at least 3 separate experiments. *$P < 0.01$, as compared to cells treated with arsenite (two-way ANOVA followed by Bonferroni's test).

Fig 4. Arsenite-dependent mitochondrial $O_2^{\cdot-}$ formation triggers mitochondrial dysfunction and apoptosis through a mechanism suppressed by AA and partially sensitive to 3-MA or Chl.

Cells were exposed to AA, Rot, 3-MA or Chl, as indicated in the legends to Figs. 1B or 3A, and subsequently treated for 16 (A) or 48 h (B-D) with arsenite. CsA was used at 0.5 µM and given to the cultures 15 min prior to addition of arsenite. Selected experiments were performed using respiration-deficient (RD) cells. After treatments, the cultures were analyzed for MitoTracker Red CMXRos-fluorescence (A), for toxicity by counting the number of viable cells (B) or for apoptosis by measuring chromatin fragmentation morphologicaly (C) or by single-cell gel electrophoresis (D). Results represent the means ± SD calculated from at least 3 separate experiments. *$P < 0.05$; **$P < 0.01$; as compared to untreated cells. (*)$P < 0.05$; as compared to cells treated with arsenite (one-way ANOVA followed by Dunnet's test).

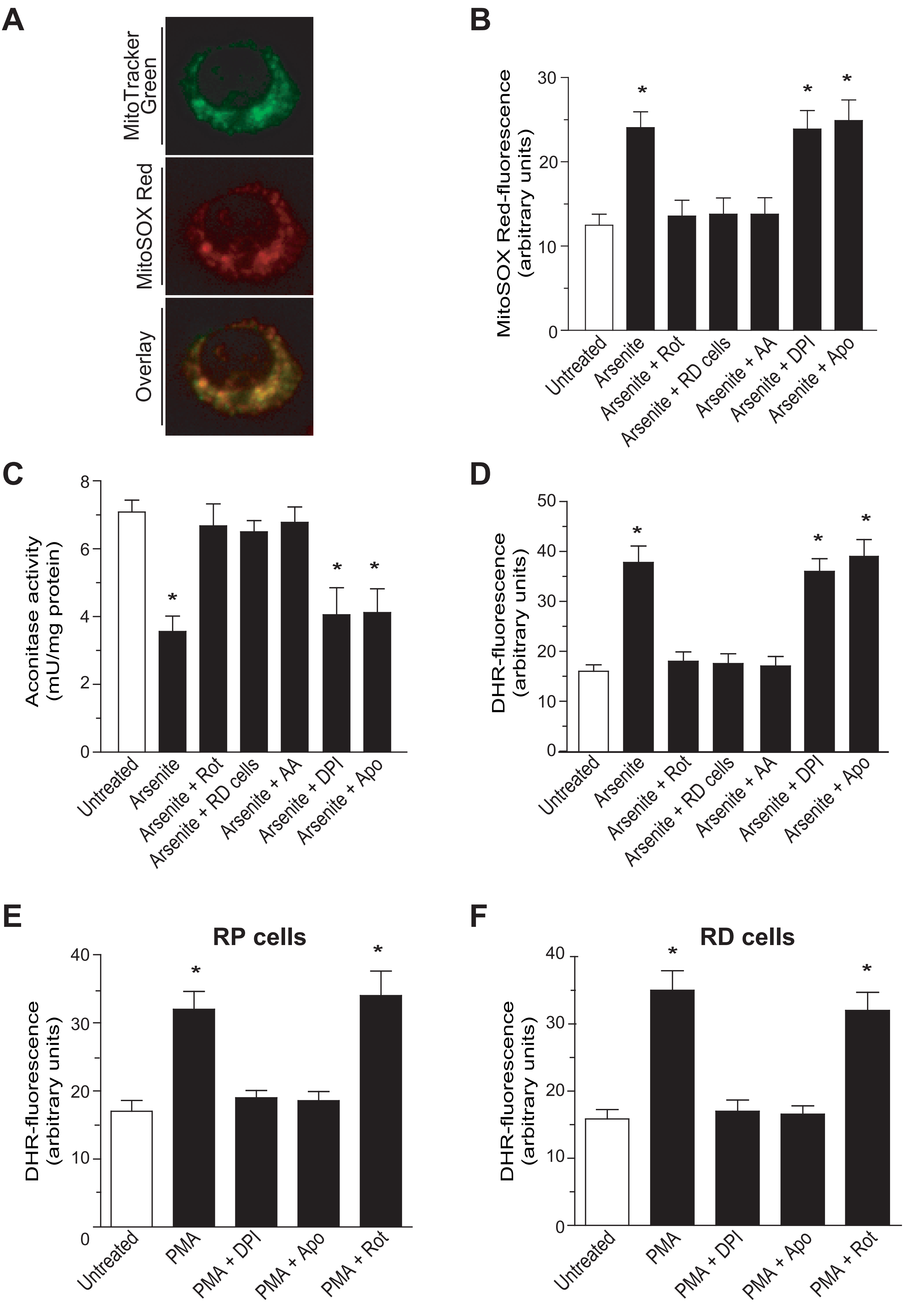
A
MitoTracker Green
MitoSOX Red
Overlay
B
MitoSOX Red-fluorescence (arbitrary units)
0
10
20
30
Untreated
Arsenite
Arsenite + Rot
Arsenite + RD cells
Arsenite + AA
Arsenite + DPI
Arsenite + Apo
C
Aconitase activity (mU/mg protein)
0
2
4
6
8
Untreated
Arsenite
Arsenite + Rot
Arsenite + RD cells
Arsenite + AA
Arsenite + DPI
Arsenite + Apo
D
DHR-fluorescence (arbitrary units)
0
10
20
30
40
50
Untreated
Arsenite
Arsenite + Rot
Arsenite + RD cells
Arsenite + AA
Arsenite + DPI
Arsenite + Apo
E
RP cells
DHR-fluorescence (arbitrary units)
0
10
20
30
40
Untreated
PMA
PMA + DPI
PMA + Apo
PMA + Rot
F
RD cells
DHR-fluorescence (arbitrary units)
0
10
20
30
40
Untreated
PMA
PMA + DPI
PMA + Apo
PMA + Rot

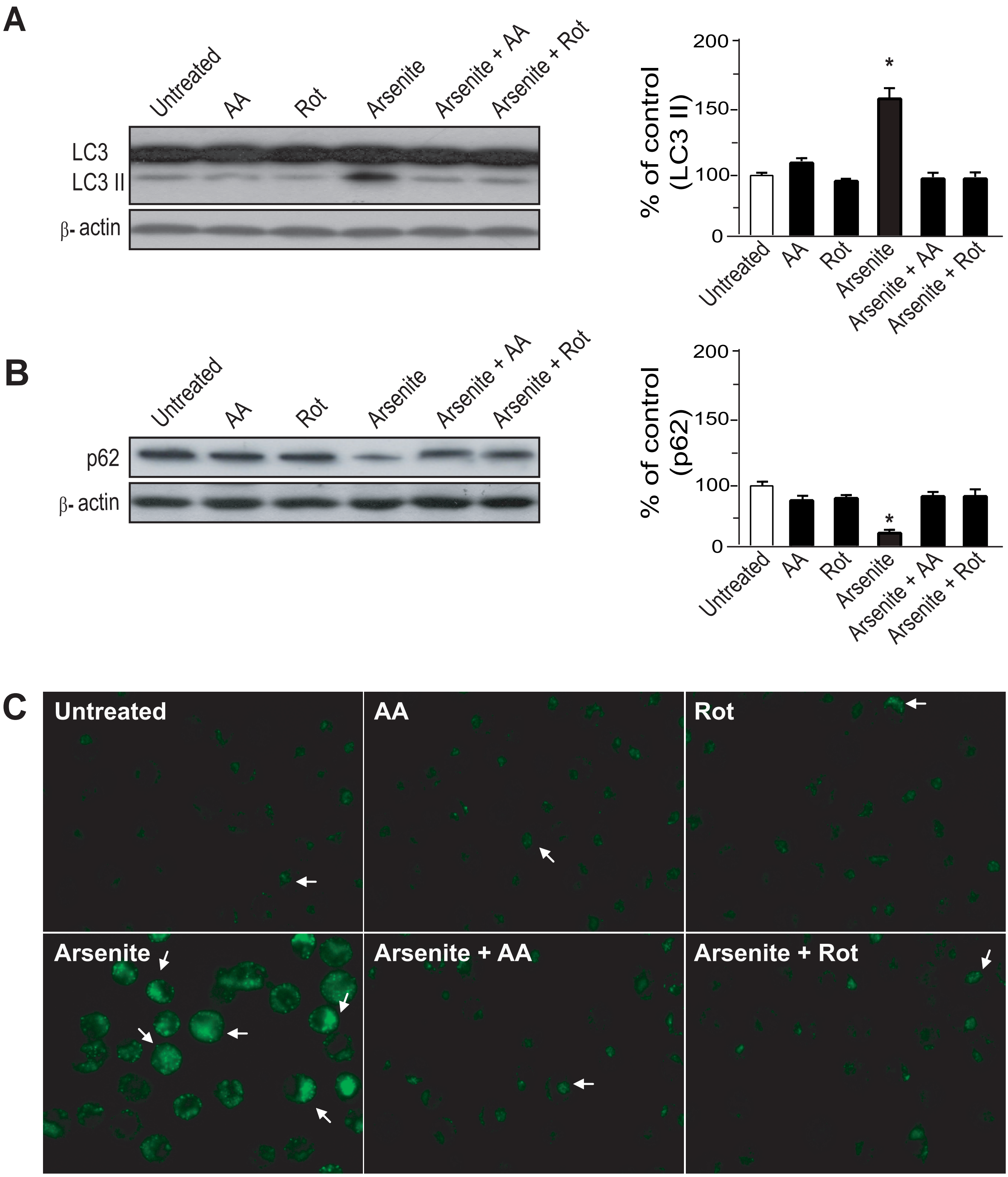
A
Untreated
AA
Rot
Arsenite
Arsenite + AA
Arsenite + Rot
LC3
LC3 II
β- actin
% of control (LC3 II)
200
150
100
0
*
B
p62
% of control (p62)
C
Untreated
AA
Rot
Arsenite
Arsenite + AA
Arsenite + Rot

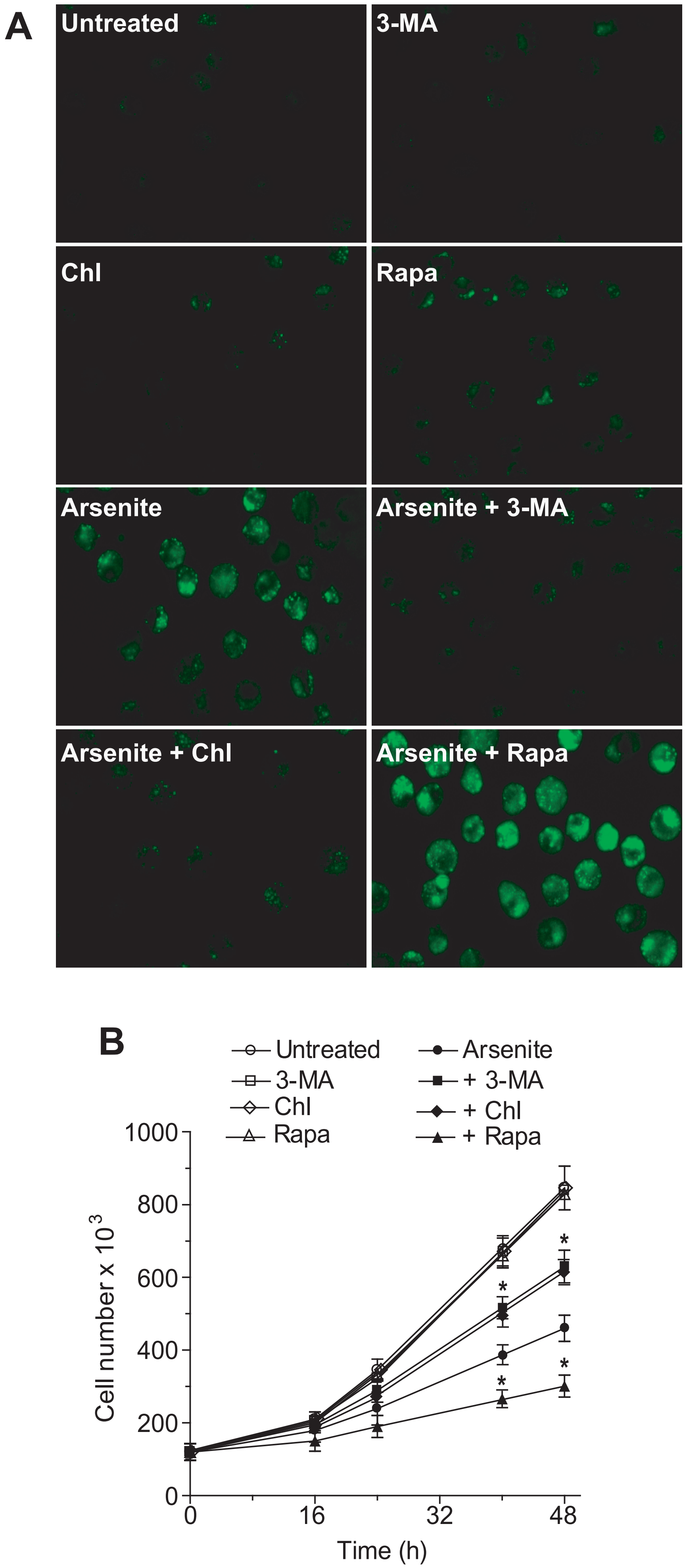

A
Untreated
3-MA
Chl
Rapa
Arsenite
Arsenite + 3-MA
Arsenite + Chl
Arsenite + Rapa
B
Untreated
3-MA
Chl
Rapa
Arsenite
+ 3-MA
+ Chl
+ Rapa
Cell number x 10^3
1000
800
600
400
200
0
0
16
32
48
Time (h)

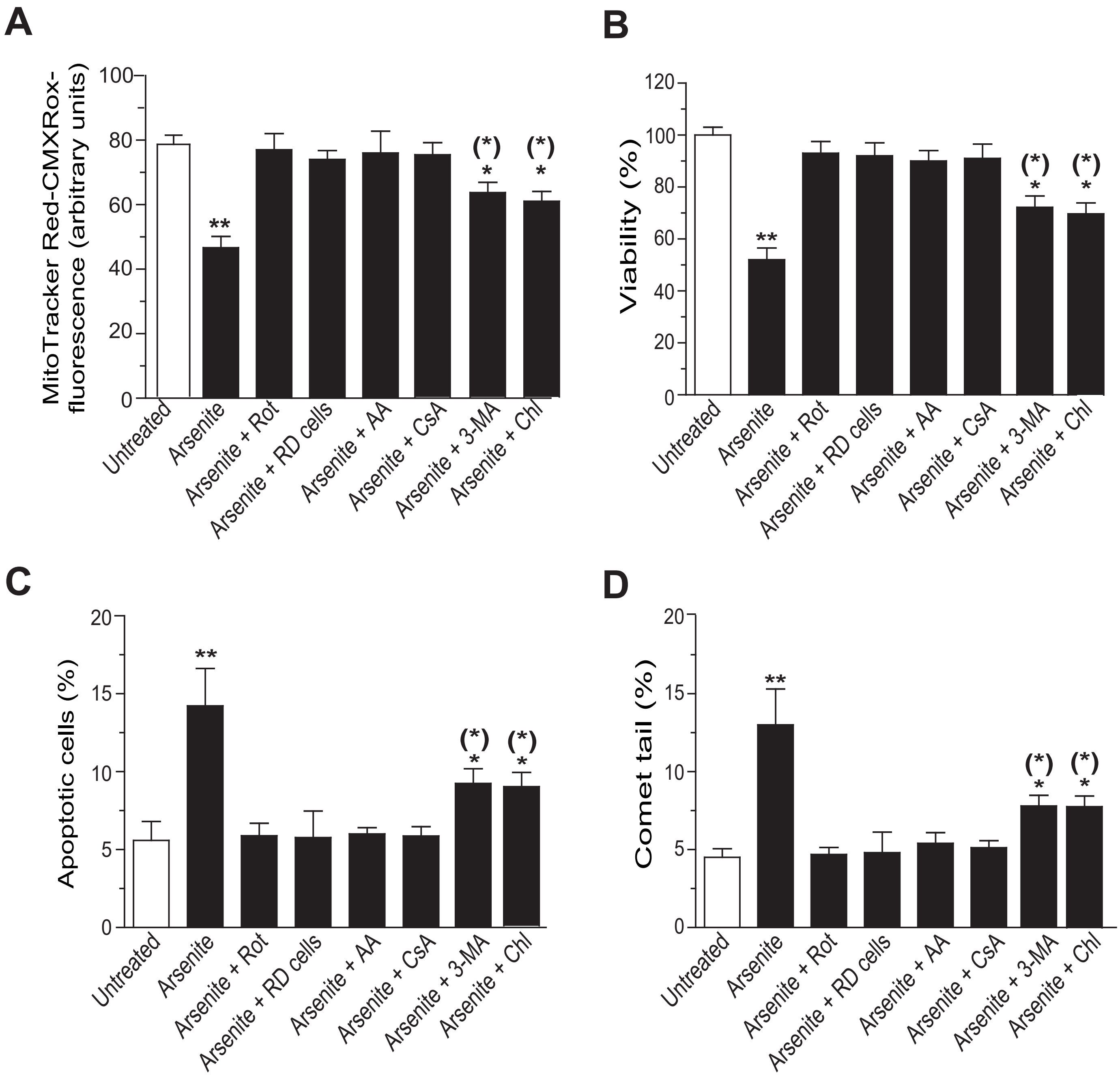
A
MitoTracker Red-CMXRox-fluorescence (arbitrary units)
100
80
60
40
20
0
**
(*)
*
(*)
*
Untreated
Arsenite
Arsenite + Rot
Arsenite + RD cells
Arsenite + AA
Arsenite + CsA
Arsenite + 3-MA
Arsenite + Chl
B
Viability (%)
120
100
80
60
40
20
0
**
(*)
*
(*)
*
Untreated
Arsenite
Arsenite + Rot
Arsenite + RD cells
Arsenite + AA
Arsenite + CsA
Arsenite + 3-MA
Arsenite + Chl
C
Apoptotic cells (%)
20
15
10
5
0
**
(*)
*
(*)
*
Untreated
Arsenite
Arsenite + Rot
Arsenite + RD cells
Arsenite + AA
Arsenite + CsA
Arsenite + 3-MA
Arsenite + Chl
D
Comet tail (%)
20
15
10
5
0
**
(*)
*
(*)
*
Untreated
Arsenite
Arsenite + Rot
Arsenite + RD cells
Arsenite + AA
Arsenite + CsA
Arsenite + 3-MA
Arsenite + Chl

Table 1. U937 cell death mediated by arsenite is caused by H_2O_2 formation

Treatment	**DHR-fluorescence (arbitrary units)**	**Viability (%)**
Untreated	15.8 ± 2.2	100 ± 2.5
Arsenite (2.5 μM)	32.4 ± 1.5*	51 ± 2.7*
+ Catalase (50 U/ml)	16.2 ± 2.1	95 ± 3.4
+ Boiled catalase	35.3 ± 1.7*	49 ± 2.8*
+ ATZ (10 mM)	54.8 ± 1.7*	25 ± 1.7*

Cells were exposed for 16 (DHR-fluorescence) or 48 h (toxicity) to 0 or 2.5 μM arsenite, with or without prior addition of various drug. After treatments, the cells were processed as indicated in the Materials and Methods section. Enzymatically active or boiled catalase were given to the cultures 15 min prior to the addition of arsenite. Results represent the means ± SD from 4 separate experiments. *$P < 0.01$ as compared to untreated cells (one-way ANOVA followed by Dunnet's test).

Table 2. U937 cell death mediated by arsenite is not caused by peroxynitrite formation.

Treatment	Immunofluorescence (arbitrary units)	Viability (%)
Untreated	14.5 ± 2.2	100 ± 3.4
Arsenite (2.5 μM)	14.8 ± 2.6	53 ± 2.4*
+ L-methionine (20 mM)	_	55 ± 1.7*
+ L-NAME (1 mM)	_	51 ± 1.9*
+ PTIO (50 μM)	_	49 ± 3.3*
Reagent peroxynitrite (100 μM)	29.4 ± 3.5*	_
+ L-methionine	15.1 ±1.2	_

Cells were exposed for 16 (nitrotyrosine immunoreactivity) or 48 h (toxicity) to 0 or 2.5 μM arsenite, with or without prior addition of various drug. In other experiments, cells were exposed for 10 min (nitrotyrosine immunoreactivity) to 0 or 100 μM peroxynitrite. After treatments, the cells were processed as indicated in the Materials and Methods section. L-methionine, L-NAME or PTIO were given to the cultures 15 min prior to the addition of arsenite or peroxynitrite. Results represent the means ± SD from 4 separate experiments. *P < 0.01 as compared to untreated cells (one-way ANOVA followed by Dunnet's test).